Journal of Bio- and Tribo-Corrosion (2020) 6:90
https://doi.org/10.1007/s40735-020-00386-3

The Multi-objective Optimization Design Approach for Carbon Fiber Hybrid Nanocomposites Containing NanoClay and NanoZnO Particles by Using OptiComp

Shailesh D. Ambekar[1] · **Vipin Kumar Tripathi**[1]

Received: 17 February 2020 / Revised: 3 June 2020 / Accepted: 17 June 2020 / Published online: 26 June 2020

Abstract
This paper presents the multi-objective design optimization of Carbon Fiber-Reinforced Polymer hybrid nanocomposites by OptiComp. The use of nanoparticles not only improves the interface strength but also significantly improves stress and hence the propagation of strain in composite laminates, which ultimately improves the stiffness of the composite laminate. The OptiComp is the comprehensive generic procedure for design optimization of the composites. With the utilization of OptiComp, the discrete form Variable thickness approach (VTA) used in this study can discover the minimum laminate thickness, and for maximum stiffness in one step instead of two-step method. The Max stress theory and Tsai-Wu theory as constraints for the current study in optimization are performed using a direct value coding genetic algorithm. It is found that the CFRP nanocomposites up to 2 to 3 wt% range of nanoparticles can be designed for max. stiffness and min. weight.

Keywords OptiComp · VTA · Nanocomposite · CFRP · Nanoclay · NanoZnO

Symbols

$\mathbf{E_{11}}$	Longitudinal direction elastic modulus
E22	Transverse directional elastic modulus
$\mathbf{G_{12}}$	Shear modulus in plane
$\mathbf{n_{12}}$	Major poisson's ratio
$\mathbf{S_{lc}}$	Longitudinal directional compressive strength
$\mathbf{S_{lt}}$	Longitudinal directional tensile strength
$\mathbf{S_{tc}}$	Transverse directional compressive strength
$\mathbf{S_{tt}}$	Transverse directional tensile strength
$\mathbf{S_{lts}}$	Shear strength
ρ	Mass density

Plate Parameters

a	Length of plate
b	Width of plate
T	Total Thickness of plate

1 Introduction

Fiber-reinforced polymer (FRP) composites have their uses in applications of engineering due to their directional stiffness and properties of high strength-to-weight ratio. The FRP nanocomposite material laminate properties can be transformed by varying the thickness by adding or removing plies, by altering the materials for matrix and fibers, and by changing the volume fraction of nanoparticles and the fiber-angle orientation. The optimization design process has been developed to find the best presentation of composite structures in a wide range of engineering applications. The design optimization can be implemented in the FRP nanocomposites [1] for the blast resistance. The combined and individual use of a genetic algorithm, finite element methods, and discrete lay-up method are effectively used by the authors in solving the optimization problems of FRP [2–5]. The design optimization of Carbon fiber-reinforced polymer and other FRP's are effectively carried out for various parts and the structures for different failure analyses and considering different parameters by Almeida, Do-Hyoung Kim, and Stacy Nelson [6–9]. G. Narayananaik et al. and Sohouli et al. have also applied the genetic algorithm for the failure creation mechanism and design optimization of the composite laminates [10, 11]. Furthermore, Yasser Rostamiyan et al. have successfully carried out experimental optimization of

✉ Shailesh D. Ambekar
sd.ambekar@gmail.com

Vipin Kumar Tripathi
vkt.mech@coep.ac.in

[1] Department of Mechanical Engineering, College of Engineering, Shivajinagar, Pune 411005, India

damping properties of nano epoxy-based composites, and high-impact polystyrene by mixture design approach by using RSM and the mechanical properties of epoxy-high-impact polystyrene/carbon multi-walled nanotubes ternary nanocomposites using an artificial genetic algorithm and neural network [12–15]. Boon et al. have also studied the comparison of wear performance of FRP nanocomposites using RSM [16]. Boroujeni et al., highlighted the improvement of mechanical properties by the implementation of carbon nanotubes in CFRP composites [17]. Abdolreza Mirmohseni et al. also successfully used RSM for modeling and optimization of nano CFRP composites [18]. Multi-objective optimization of the composite FRP laminates was studied by various researchers for different automobile components and structures [19–21]. Pelletier et al. have explored a study on the maximization of the stiffness, strength, and for minimal mass [22]. Many researchers have focused on the optimization of flexural strength, stacking sequence, and cost optimization of FRP composites [23–25]. Narayana Naik et al. have used the optimization technique by nature-inspired in designing composite structures [26]. Rahul et al. have optimized the impact strength of FRP laminates by using the island model parallel genetic algorithm [27]. Some of the researchers have continued their study on optimizing by considering different failure criteria, flexural properties of nanocomposites by using RSM, and optimization of variable stiffness composites [28–30]. Jie et al. optimized the tribological properties of fiber and matrix interface [31]. Meera Balachandran et al. have implemented the CCD method for the optimization of nanocomposites [32]. Optimization of the delamination failure, buckling load capacity, and minimal thickness is carried out in the studies of many researchers [33–35]. Srinivas et al. have studied the effect of carbon nanotubes on various properties of nanocomposites [36]. Chung Park et al. have done their study on optimization of composite structures by considering manufacturing cost and mechanical performance [37]. Tripathi et al. have developed a comprehensive optimization procedure named as OptiComp. This method can be effectively used for multi-objective optimization of FRP laminate design by considering the VTA and uniform thickness approach as well. They have considered ply orientation angle, thickness, the density of the material, etc. as the variables/parameters and the Tsai-Wu, Tsai–Hill, and Maximum stress theories of failure as constrains. The OptiComp seems to be a very useful tool in implementing the design optimization of plain FRP/FRP hybrid nanocomposites [38–40]. Leila Fakhri et al. have explored their study on polystyrene nanoclay and nanoZnO composite by RSM [41]. Balaji has studied the morphological and mechanical properties of banana FRP composites.

In the current study, the multi-objective design optimization of the CFRP hybrid nanocomposites containing nanoclay and nanoZnO particles was done by using OptiComp. The use of nanoparticles not only improves the strength of the interface but also significantly alters stress and strain propagation in composite laminates which ultimately improves in the stiffness of CFRP composite laminates.

2 Material and Methods

2.1 Materials

In the current study, the Control sample was carbon fiber-reinforced polymer (CFRP) composites. The carbon fiber of 200 GSM, standard modulus of 3K, and HCU200 code is used for the main reinforcement. Hinpoxy C epoxy resin is Bisphenol-A-based liquid-state material. HARDENER-B is a modified amine hardener, has low viscosity, and is a colorless liquid, with a stoichiometric ratio of A:B = 10:3; the fiber and the resin both were supplied by the Hindoostan Mills Ltd. Mumbai, India. NanoZnO particles and montmorillonite nanoclay were used, supplied by Nano Research Lab. Jamshedpur, (Jharkhand), India. All the details of the properties are given in Table 1.

Table 1 Material properties

Properties	Value
Properties of carbon fiber	
Density (g/cm^3)	1.8
Tensile Strength (MPa)	4000
Elongation (%)	1.7
Filament diameter (μm)	7
Tensile modulus (GPa)	240
Properties—hinpoxy C resin	
Viscosity at 25 °C, mPas	9000–12,000
Density at 25 °C, g/cc	1.15–1.20
Flash point, 0X	> 200
Properties—hinpoxy C hardener	
Viscosity at 25 °C, mPas	< 50
Density at 25 °C, g/cc	0.94 –0.95
Flash Point, 0X	> 123
NanoZnO properties	
Purity	99.9%
SSA	20–60 m^2/g
Morphology	Nearly spherical
True density	6 g/cm^3
Average particle size	30–50 nm
Color	Milky white
Bulk density	0.28–0.48 g/cm^3
Nanoclay properties	
Purity	99.9%
stack size	5–10 μm
Bulk density	37 to 56 lbs./f^{t3}

2.2 Sample Fabrication

The carbon fiber-reinforced polymer nanocomposite laminates were manufactured by the process of hand lay-up method, followed by the process of vacuum bagging. Here, the main part of the reinforcement was unidirectional carbon fiber in the epoxy resin. Bisphenol A (DGEBA) resin was mixed up with hardener in the ratio of 100:30 of weight. The clay and Zinc Oxide nanoparticles were used as a nanofillers. For the suitable dispersion in the epoxy resin clay and Zinc Oxide Nanoparticles, first of all, nanoparticles were dried before use overnight at 75^0C in an oven. For the attainment of a uniform dispersion of the nanoclay and ZnO(Zinc Oxide) nanoparticles in the epoxy resin, the magnetic stirring and ultrasonication process of the mixture were carried. The % weight of nanoparticle content was used in the range of 1% to 5% in the mixture of the epoxy resin and hardener as per the results from OVAT analysis and previous research carried out. Ultra-sonication bath method was then carried out for 40 min at 40° C for uniform mixing of the nanoparticles in the epoxy resin. After ultrasonication, the prepared mixture was then magnetically stirred for around one and a half hours. The prepared mixture was used for the CFRP nanocomposite preparation. The hand lay-up-prepared sample is then followed by the process of vacuum bagging which was carried out for 4.5–5 h with a constant vacuum pr. of 720 mmHg. Fourteen plies were used, and according to the coded levels, the combination of three factors was varied. The specimen was kept in the bag for 15–18 h at room temperature for curing. The post-curing of the specimen was then done in an oven for five hours at 80 °C.

2.2.1 OptiComp

OptiComp is the comprehensive generic procedure for the design optimization of composites. With the implementation of the OptiComp, the discrete form Variable thickness approach (VTA) used in this study can find the minimum laminate thickness, and for maximum stiffness in one step instead of two-step methodology. The required laminate minimum thickness can be used by the designer in several ways. The present study found that the effect of the Variable thickness approach (VTA) in this regard is dependent on the ply thickness increment value and the ply number. Tsai-Wu theory and Maximum stress theory were used as constraints for a given loading condition. Ply angle, ply thickness, and ply number are used as a design variable in the current simulation study in discrete form. Optimization is performed using a direct value coding genetic algorithm. You can choose two approaches for designing composite laminates, i.e., Variable Thickness Approach (VTA) and Uniform Thickness Approach (UTA). In UTA, all plies are of uniform thickness, and ply angles and multiple plies are treated as design variables. In VTA, ply angle, ply count, and ply thickness are treated as design variables. In the new process, OptiComp, the following change has been made in conventional GA to costume the problem of composite laminate design optimization.

(i) Instead of binary-coded representation. Direct value-coded representation is used for chromosomes.

This type of representation gives ease in handling of multiple design variables of different nature in discrete form.

(ii) The direct value-coded chromosome demonstration can accurately catch increment value for the design variables given by the user within the limit bounds, which is hard in binary representation.

(iii) The single-point crossover mutation/function is defined in such a way to suit the chromosome representation. The chromosome representation and cross-over mutation for the new procedure OptiComp are shown in Fig. 1.

2.2.2 Maximum Stress Theory

According to the given theory of failure, a composite lamina will fail, when the value of any one of the principal stresses created in the lamina equalizes its limiting value. The limiting values are defined by their respective strengths. The lamina will fail, if

$$\sigma_{11} = \mathrm{S_{LC}} \text{or} \sigma_{11} = \mathrm{S_{Lt}} \tag{1}$$

$$\sigma_{22} = \mathrm{S_{TC}} \text{or } \sigma_{22} = \mathrm{S_{Tt}} \tag{2}$$

$$\tau_{12} = \mathrm{S_{Lts}},$$

where σ_{11} and σ_{22} are normal stresses created in directions 1 and 2, respectively, while $\tau 12$ is the shear stress developed in plane 1–2 for individual lamina.

2.2.3 Tsai-Wu Theory (TW)

Based on the von Mises yield criterion, according to this theory, the lamina under the consideration will fail, when the below-mentioned condition is satisfied.

$$F_1\sigma_{11} + F_2\sigma_{22} + F_6\tau_{12} + F_{11}\sigma_{11}^2 + F_{22}\sigma_{22}^2 + F_{66}\tau_{12}^2 + 2F_{12}\sigma_{11}\sigma_{22} = 1,$$

where F_1,F_2,F_6,F_{11}, F_{22}, F_{66}, and F_{12} are the coefficients which can be calculated using strengths of the lamina in different directions as given below,

$$F_1 = \frac{1}{S_{\mathrm{Lt}}} - \frac{1}{S_{\mathrm{LC}}}, F_2 = \frac{1}{S_{\mathrm{Tt}}} - \frac{1}{S_{\mathrm{TC}}}, F_6 = 0$$

$$F_{11} = \frac{1}{S_{\mathrm{Lt}}S_{\mathrm{LC}}}, F_{22} = \frac{1}{S_{\mathrm{Tt}}S_{\mathrm{TC}}}, F_{66} = \frac{1}{S_{\mathrm{Lts}}^2}, F_{12} = -\frac{1}{2}\left(F_{11}F_{12}\right)^{0.5}$$

A suitable biaxial test is required for determining F_{12} is

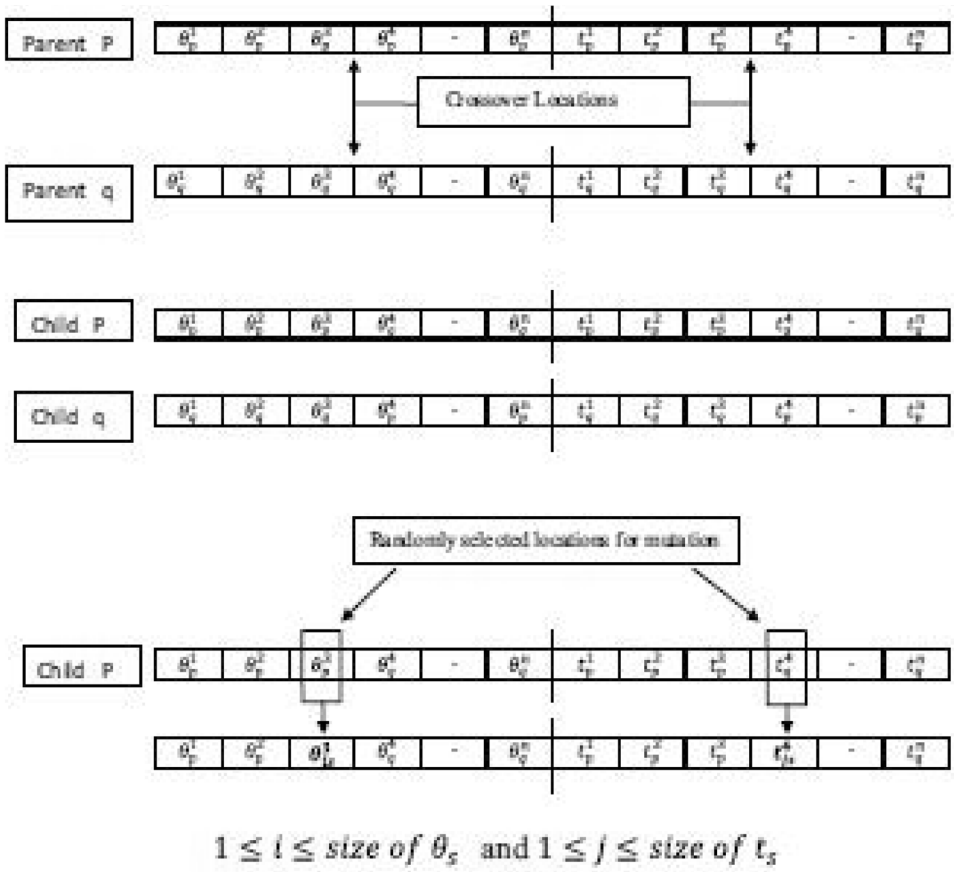

Fig. 1 Chromosome representation, crossover, and mutation in OptiComp

$$-\frac{1}{2}\left(F_{11}F_{12}\right)^{0.5} \le F_{12} \le 0$$

In the absence of any experimental data, the lower limit of the above equation is frequently used as F_{12}.

3 Generalized Problem Domain

Using the classical lamination plate theory, the strains and stresses developed in each lamina are calculated. The geometry of the laminate coordinate systems and loading conditions considered in the analysis are shown in Fig. 2. The geometric parameters necessary for the laminate analysis are shown in Fig. 3.

4 Inputs:

- Plate Dimensions (Length and Width)
- Loading Conditions (N_{xx}, N_{yy}, N_{xy})
- Material Properties (Elastic Properties, Poisson's Ratio, Strengths)
- Maximum number of Plies

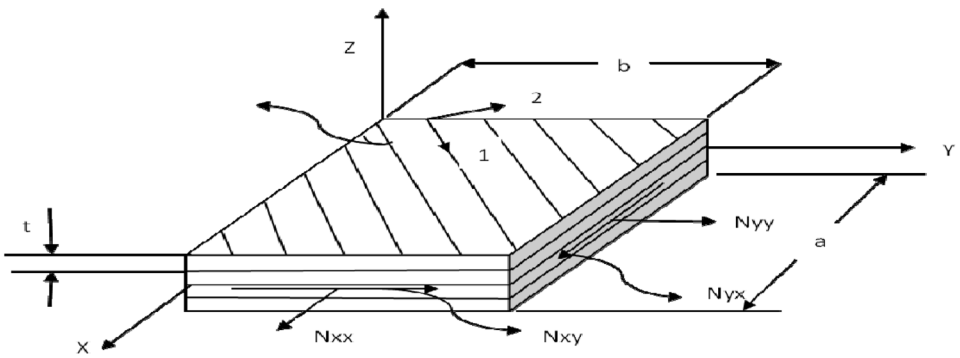

Fig. 2 Global and local coordinate systems for composite laminate

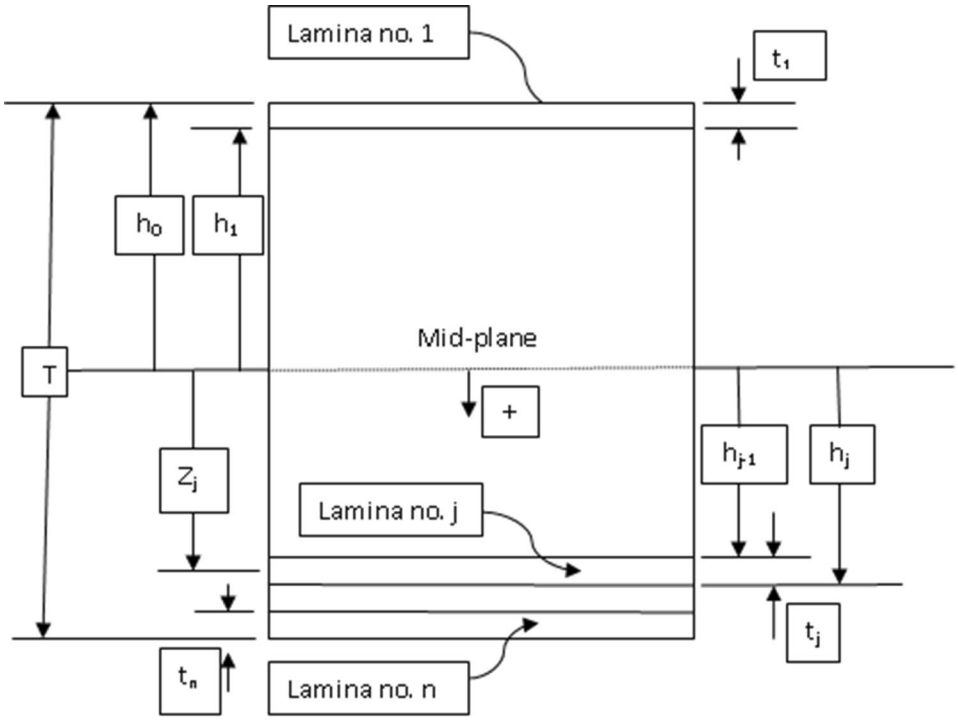

Fig. 3 Laminate geometric properties

The elements of $\left[\overline{Q}\right]$ the stiffness matrix can be developed from the material properties

$$\left[\overline{Q}_{mn}\right] = \begin{bmatrix} \overline{Q}_{11} & \overline{Q}_{12} & \overline{Q}_{16} \\ \overline{Q}_{12} & \overline{Q}_{22} & \overline{Q}_{26} \\ \overline{Q}_{16} & \overline{Q}_{26} & \overline{Q}_{66} \end{bmatrix}$$

The elements of $\left[\overline{Q}\right]$ the stiffness matrix can be calculated as

$$\overline{Q}_{11} = Q_{11}\cos^4\theta + 2\left(Q_{12} + 2Q_{66}\right)\sin^2\theta\cos^2\theta + Q_{22} \quad (3)$$

$$\overline{Q}_{12} = Q_{12}\left(\sin^4\theta + \cos^4\theta\right) + \left(Q_{11} + Q_{22} - 4Q_{66}\right)\sin^2\theta\cos^2\theta \quad (4)$$

$$\overline{Q}_{22} = Q_{11}\sin^4\theta + 2\left(Q_{12} + 2Q_{66}\right)\sin^2\theta\cos^2\theta + Q_{22}\cos^4\theta \quad (5)$$

$$\overline{Q}_{16} = \left(Q_{11} - Q_{12} - 2Q_{66}\right)\sin\theta\cos^3\theta + \left(Q_{12} - Q_{22} + 2Q_{66}\right)\cos\theta\sin^3\theta \quad (6)$$

$$\overline{Q}_{26} = \left(Q_{11} - Q_{12} - 2Q_{66}\right)\cos\theta\sin^3\theta + \left(Q_{12} - Q_{22} + 2Q_{66}\right)\sin\theta\cos^3\theta \quad (7)$$

$$\overline{Q}_{66} = \left(Q_{11} + Q_{22} - 2Q_{12} - 2Q_{66}\right)\sin^2\theta\cos^2\theta + Q_{66}\left(\sin^4\theta + \cos^4\theta\right), \quad (8)$$

where $Q_{11} = \frac{E_{11}}{1-\gamma_{12}\gamma_{21}}$, $Q_{22} = \frac{E_{22}}{1-\gamma_{12}\gamma_{21}}$, $\gamma_{21} = \gamma_{12}\frac{E_{22}}{E_{11}}$.

$Q_{12} = Q_{21} = \frac{\gamma_{21}E_{11}}{1-\gamma_{12}\gamma_{21}} = \frac{\gamma_{12}E_{22}}{1-\gamma_{12}\gamma_{21}}$, $Q_{66} = G_{12}$.

The additionally required geometric parameters for the laminate analysis are shown in Fig. 3, t_1, t_j, and t_n indicate 1st, *j*th, and nth thicknesses of laminates; h0 gives space from the mid-plane laminate to the top of the 1st lamina, while h_1 indicates the space/distance from the mid-plane laminate to the bottom of the 1st lamina. h_{j1} specifies the distance between the top to laminate mid-plane of the *j*th lamina and h_j indicates the distance from the bottom to the mid-plane of laminate the *j*th lamina. The entire thickness of the laminate is specified by with letter T_{Zj} gives the distance from the mid-plane laminate to the mid-plane of the *j*th lamina

$[A_1] = [A^{-1}] + [A^{-1}]\,[B]\,[(D^*)^{-1}]\,[B]\,[A^{-1}]$.

$[B_1] = -[A^{-1}]\,[B]\,[(D^*)^{-1}]$, $[C_1] = [B_1]^T$.

$[D^*] = [D] - [B]\,[A^{-1}]\,[B]$, $[D_1] = [(D^*)^{-1}]$.

The curvatures [K] and mid-plane strains $[\varepsilon^0]$ can be calculated as

$$[\varepsilon^0] = [\mathrm{A}_1][\mathrm{N}] + [\mathrm{B}_1][\mathrm{M}] \text{ where} \tag{9}$$

$$\left[\varepsilon^0\right] = \begin{bmatrix} \varepsilon^0_{xx} \\ \varepsilon^0_{yy} \\ \varepsilon^0_{xy} \end{bmatrix}, \ [\mathrm{N}] = \begin{bmatrix} N_{xx} \\ N_{yy} \\ N_{xy} \end{bmatrix}, \ [M] = \begin{bmatrix} M_{xx} \\ M_{yy} \\ M_{xy} \end{bmatrix}$$

$$[\mathrm{K}] = [\mathrm{C}_1][\mathrm{N}] + [\mathrm{D}_1][\mathrm{M}] \tag{10}$$

The curvatures and strains at the mid-plane are used to calculate actual stresses and strains for individual lamina in global coordinate system.

$$[\varepsilon]_j = \left[\varepsilon^0\right] + Z_j[\mathrm{K}] \tag{11}$$

The converted local coordinate system from the global one, for individual lamina.

Can be given by using the relations given below.

$$\varepsilon_{11} = \varepsilon_{xx}\cos^2\theta + \varepsilon_{yy}\sin^2\theta + \varepsilon_{xy}\sin\theta\cos\theta \tag{12}$$

$$\varepsilon_{22} = \varepsilon_{xx}\sin^2\theta + \varepsilon_{yy}\cos^2\theta - \varepsilon_{xy}\sin\theta\cos\theta \tag{13}$$

$$\varepsilon_{12} = 2(-\varepsilon_{xx} + \varepsilon_{yy})\sin\theta\cos\theta + \varepsilon_{xy}\cos^2\theta - \sin^2\theta$$

$$[\sigma]_j = \left[\overline{Q}\right]_j [\varepsilon]_j \text{ where } [\sigma] = \begin{bmatrix} \sigma_{xx} \\ \sigma_{yy} \\ \tau_{xy} \end{bmatrix} \tag{14}$$

whereZ_j is the space/distance from the mid-plane laminate to the mid-plane of the *j*th lamina.

The local converted coordinate system from global stresses, for individual lamina, can be given.

By using the relations below.

$$\sigma_{11} = \sigma_{xx}\cos^2\theta + \sigma_{yy}\sin^2\theta + 2\tau_{xy}\sin\theta\cos\theta \tag{15}$$

$$\sigma_{22} = \sigma_{xx}\sin^2\theta + \sigma_{yy}\cos^2\theta - 2\tau_{xy}\sin\theta\cos\theta \tag{16}$$

$$\tau_{12} = (-\sigma_{xx} + \sigma_{yy})\sin\theta\cos\theta + \tau_{xy}\cos^2\theta - \sin^2\theta \tag{17}$$

The second approach 'Ideal Procedure' for solving MOOP is developed on the basis of Non-Dominated Sorting G.A. (NSGA II) in the generic procedure (Refer Fig. 4). In NSGAII, the P_t population of the parent is used to create the offspring population Q_t. During this process, the genetic operators like crossover, selection, and mutation are applied to the population of the parent P_t. Then two populations are combined to create the R_t population. If 'N' is the size of the parent population, then the size of R_t will be '2 N.' Then by using a non-dominated

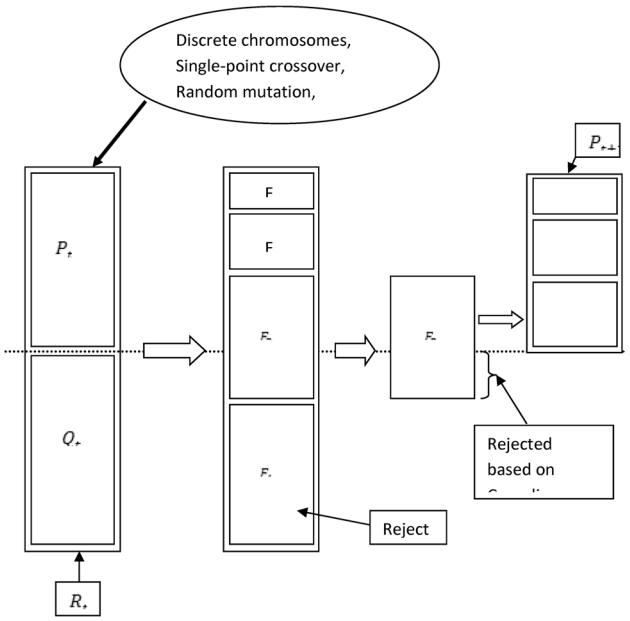

Fig. 4 Flowchart of Non-Dominated Sorting G.A. (NSGA II) in the generic procedure

sorting procedure, the entire population R_t is classified. This allows a non-domination global check among the off spring and parent solutions. After this step, solutions from different non-dominated fronts are used one by one to fill P_{t+1} the new population. The filling starts through the finest non-dominated front and continues by way of solutions of the second non-dominated front, succeeded by the third one and so on. As the size of the new population is 'N,' it cannot occupy all the solutions from the overall population R_t of size '2 N.' The fronts going beyond size 'N' could not be accommodated and so are deleted. The allowed last front may include extra solutions than the existing slots/space in the population new one. In such a situation, crowd sorting of the solutions explained below is used to choose the member of the last front, which is placed in the least crowded region of that front.

Crowded tournament selection: A solution 'i' is declared as tournament winner with another solution 'j' if any of the following conditions are satisfied.

1. If the solution 'i' has better rank, i.e., $r_i < r_j$
2. For the same ranks, solution 'i' must have a better crowding distance than solution 'j.'

The solutions from the same front will carry the same rank. At this stage, the second criterion is more important. The newly formed population P_{t+1} can be used for developing new offspring population Q_{t+1}., this will complete one generation of NSGAII. This process is explained in Fig. 4. The generic procedure is developed using Matlab, which has

its multi-objective optimization toolbox. NSGAII under the multi-objective optimization toolbox of the Matlab considers all the design variables in continuous form. The practically available values of ply angles and ply thicknesses are in discrete form. In a multi-objective optimization module based on NSGAII, the parent population P_t is generated considering the user-required ply thickness and ply angle values. The nature of the chromosomes developed is similar to as mentioned in Fig. 1 for VTA and UTA. The selection operator is adopted from the Matlab toolbox, which is based on the selection method of the tournament. The single-point crossover and mutation operators as defined in Fig. 1 are applied to this population to the general population Q_t.

By default, the Matlab MOOP toolbox is not meant to accept non-linear constraints for the 'custom' population used in the process. The non-linear constraints in the case of composite laminate design are the different theories of failure. The non-linear constraints are invoked in the NSGAII-based module developed under OptiComp using the penalty approach.

4.1 Problem Variables Within the Project Domain

Objectives:

(i) Maximize stiffness
(ii) Minimize weight

Design variables:

(i) Type of fiber
(ii) Fiber orientation angle
(iii) Thickness of lamina
(iv) Number of laminae
(v) wt% of nanoparticles

Constraints:

(i) Maximum stress theory
(ii) Tsai-Wu theory

4.2 Formulation of Problem

Find $\{\theta_n, t_n\}$,

To minimize the weight,

$$W = \rho.a.b.T \quad \left(T = \sum_{i=1}^{n} t_i\right) \tag{18}$$

To maximize the stiffness or to minimize the strain,

$$K_{xx} \propto \frac{1}{\varepsilon_{xx}}$$

$$K_{yy} \propto \frac{1}{\varepsilon_{yy}}$$

$$K_{xy} \propto \frac{1}{\varepsilon_{xy}} \tag{19}$$

Subjected to satisfying

Maximum stress theory and Tsai-Wu theory
$-45° \geq \theta_n \geq 90°$ (Ply angle incremental value 15°),
$0.2 \leq t_n \leq 0.4$ (Ply thickness incremental value 0.01 mm),
$n = 1,\ldots, N_{\max}$ ($N_{\max}$ as obtained in an earlier stage).

The values used in the OptiComp, calculated by mixture rule and measured by the testing

The rule of the mixture is as given below

$$E_L = E_f V_f + E_m V_m = E_f V_f + E_m(1 - V_f) = E_m + V_f(E_f - E_m) \tag{20}$$

The values represented in Table 2 are calculated by using the law of mixture as shown in the equation above the Table. The values of the tensile strength in the longitudinal and transverse direction given in Table 1 are obtained from the experimental results.

Table 2 Calculated and experimental values of the parameters used in OptiComp

wt% of nanoZnO	wt% of nanoclay	CFRP/Nano mat Combination	E_1Gpa	E_2Gpa	G_{12}Gpa	n_{12}	S_{lc}Mpa	S_{lt}Mpa	S_{tc}Mpa	S_{tt} Mpa	S_{lts} Mpa	ρ gm/cm^3
0	0	Pure CFRP	65	4.57	21.40	0.226	1142	**757.05**	170	**70**	60	1.171
2	2	Level I	70.52	10.56	21.58	0.228	1142	**971**	170	**67.76**	60	1.214
2	3	Level II	74.71	13.39	21.83	0.230	1142	**798**	170	**70**	60	1.233
3	2	Level III	73.74	11.24	21.86	0.230	1142	**732.90**	170	**70**	60	1.236
3	3	Level IV	75.71	14.05	21.89	0.230	1142	**764.12**	170	**68.54**	60	1.246
2	4	Level V	74.44	15.95	21.65	0.230	1142	**885.14**	170	**75.14**	60	1.233
4	2	Level VI	72.44	11.66	21.70	0.224	1142	**625**	170	**62**	60	1.242

5 Result and Conclusions

As per the results obtained from the OptiComp as shown in Tables 2 and 3, we can get the different minimum and maximum values of the weights and the stains of the laminates at the different combinations of the nanoparticles and CFRP. The comparison of the different level weights and strains at both the theories of failure as a constraint can be easily obtained from the given tables.

As per the values given in Tables 3 and 4, the graphs are shown in Figs. 5, 6, 7, and 8. It displays the different levels and behavior of the material system of different combinations of the nanoparticles combination, i.e., nanoclay and nanoZnO percentage mixture with the CFRP.

Table 3 Showing the result of Minimum and Maximum weight and strain range for Max stress Theory as a constraint

wt% of nanoZnO	wt% of nanoclay	CFRP/Nano mat Combination	Wt in gms for Max stress Theory as a constraint		Strain in mm for Max stress Theory as a constraint	
			MinWt	MaxWt	Min Strain	Max strain
0	0	Pure CFRP	3.59029	5.65593	0.0068681	0.010537
2	2	Level I	3.73783	5.65593	0.0061653	0.009329
2	3	Level II	3.46122	5.6826	0.0060841	0.009988
3	2	Level III	3.56454	5.78592	0.0060540	0.009826
3	3	Level IV	3.85392	5.83296	0.0058965	0.008924
2	4	Level V	3.8745	5.21766	0.0066503	0.008955
4	2	Level VI	4.32264	5.57256	0.0064506	0.008315

Table 4 Showing the result of Minimum and Maximum weight and strain range for Tsai-Wu Theory as a constraint

wt% of nanoZnO	wt% of nanoclay	CFRP/Nano mat Combination	Wt in g for Tsai-Wu Theory as a constraint		Strain in mm for Tsai-Wu Theory as a constraint	
			MinWt	MaxWt	Min Strain	Max strain
0	0	Pure CFRP	3.59029	5.60675	0.0067476	0.010537
2	2	Level I	3.20166	5.69184	0.0063305	0.01125453
2	3	Level II	3.20624	6.09588	0.0056716	0.0104571
3	2	Level III	3.8745	5.83758	0.0060005	0.0090407
3	3	Level IV	3.43728	5.4684	0.0062896	0.0100063
2	4	Level V	3.51288	5.32098	0.0065211	0.0098775
4	2	Level VI	4.1664	5.88504	0.006108	0.0086277

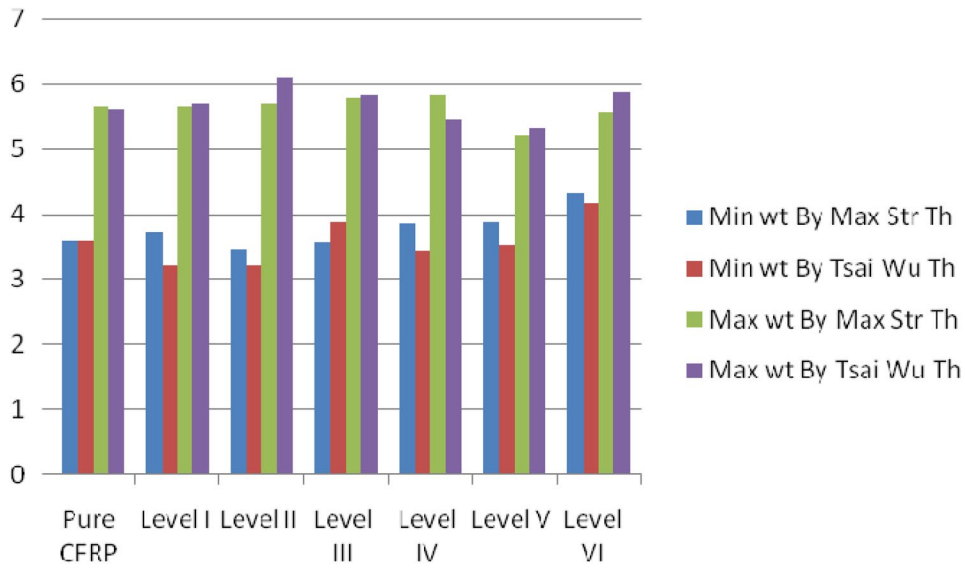

Fig. 5 Bar chart showing the maximum and minimum weight for various levels of CFRP hybrid nanocomposites

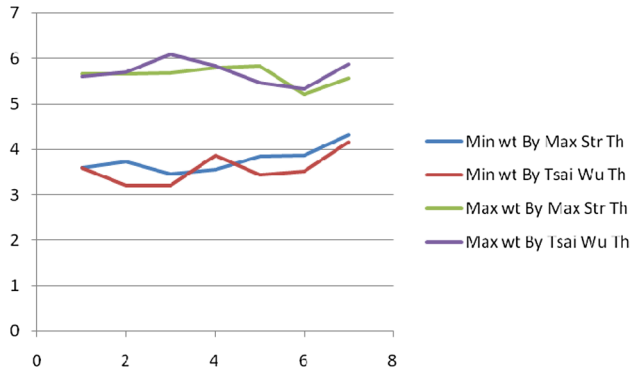

Fig. 6 Line chart showing the maximum and minimum weight for various levels of CFRP hybrid nanocomposites

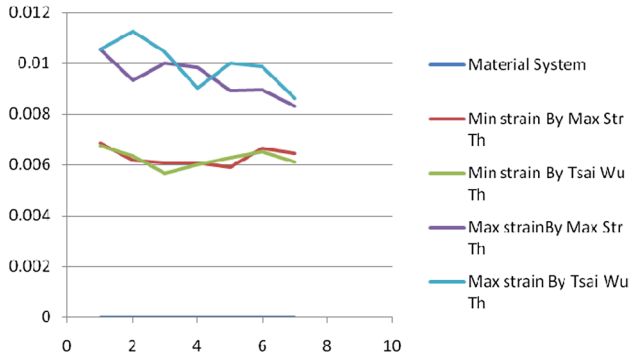

Fig. 8 Line chart showing the maximum and minimum strain for various levels of CFRP hybrid nanocomposites

Fig. 7 Bar chart showing the maximum and minimum strain for various levels of CFRP hybrid nanocomposites

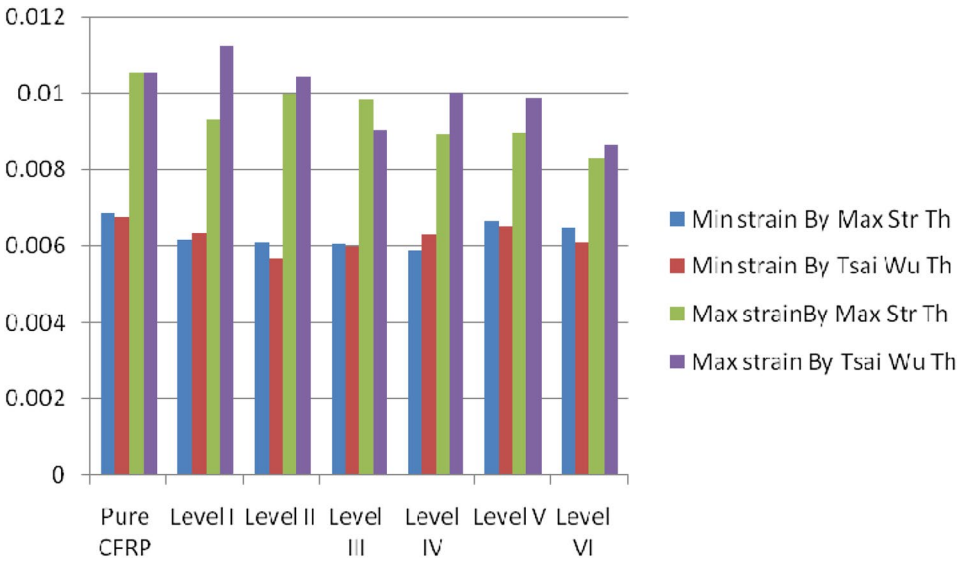

From the Pareto, optimal fronts are the multi-objective OptiComp results for the pure CFRP and new CFRP material systems with the nanoparticles shown in Fig. 9a–g for the Maximum stress theory as a constraint and Fig. 10a–g for the Tsai-Wu theory as the constraint. The simultaneous sample readings of stacking sequence angles and corresponding thickness of the laminas are as shown in Tables 5 and 6, respectively.

It can be observed from the Pareto charts and the readings of the Table 3, for the Maximum stress theory as constraint, the minimum weight of the laminate is going to be obtained at Level II, i.e., CFRP with 2 wt% of nanoZnO and 3 wt% of nanoclay. Simultaneously at Level –IV, we can observe the minimum strain, i.e., maximum stiffness of the material system with 3% each wt of Nanoclay and nanoZnO with CFRP. We can get the optimum results between 2 and 3% of both nanoclay and nanoZnO. We can also observe from Table 4 and corresponding Pareto optimal fronts, with Tsai-Wu theory as a constraint. The minimum weight for the CFRP hybrid nanocomposite can be obtained at Level I with 2 wt% of nanoparticles of each of clay and ZnO. The maximum stiffness can be obtained with Level II with 2 wt% of nanoclay and 3 wt% of ZnO nanoparticles. Tables 5 and 6 show the sample of the stacking sequence and thickness of the respective layer of the laminates for the respective theories as constraints. From the foresaid graphs and the results, it can be proved that the OptiComp can be effectively and efficiently used for solving the multi-objective design optimization problems related to FRP hybrid nanocomposites.

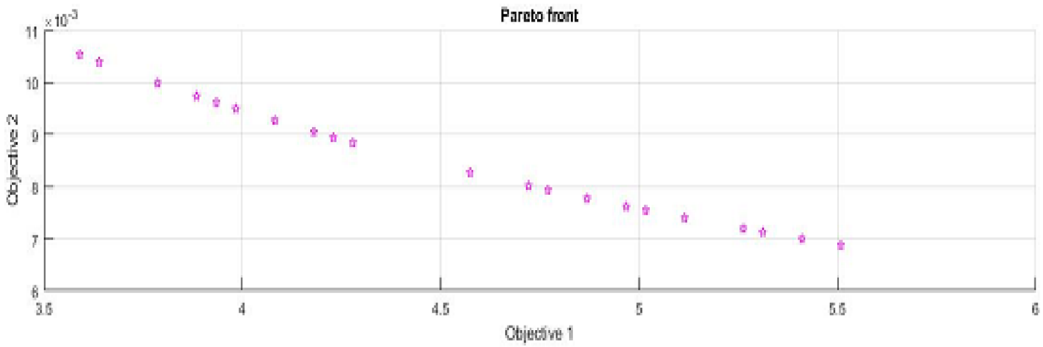

(a) Pareto optimal front for Pure CFRP composite laminate for Max stress Th

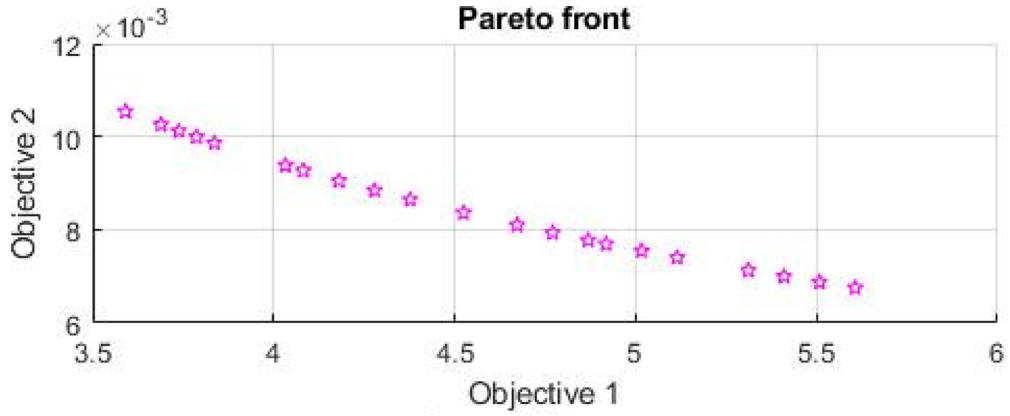

(b) Pareto optimal front for Level –I CFRP nanocomposite laminate for Max stress Th

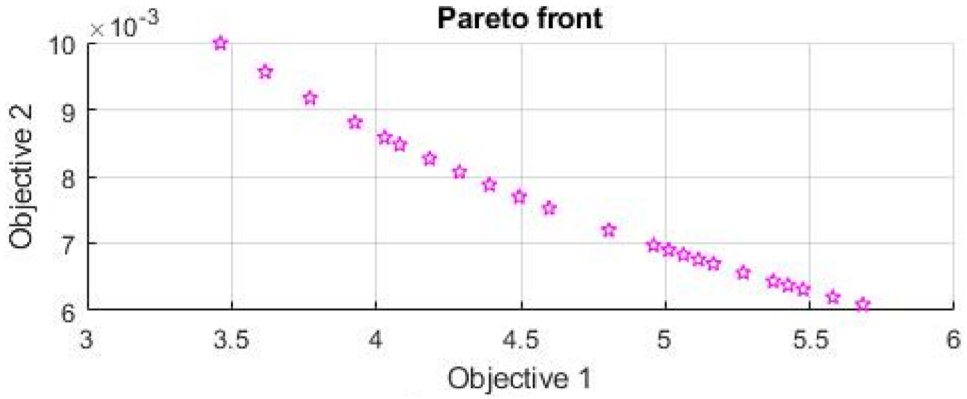

(c) Pareto optimal front for Level –II CFRP nanocomposite laminate for Max stress Th

Fig. 9 **a**–**g** Pareto optimal front for various levels of CFRP hybrid nanocomposite for Max. Stress theory as a constraint. **a** Pareto optimal front for Pure CFRP composite laminate for Max stress Th. **b** Pareto optimal front for Level-I CFRP nanocomposite laminate for Max stress Th. **c** Pareto optimal front for Level-II CFRP nanocomposite laminate for Max stress Th. **d** Pareto optimal front for Level-III CFRP nanocomposite laminate for Max stress Th**. e** Pareto optimal front for Level-IV CFRP nancomposite laminate for Max stress Th. **f** Pareto optimal front for Level-V CFRP nanocomposite laminate for Max stress Th. **g** Pareto optimal front for Level-VI CFRP nanocomposite laminate for Max stress Th

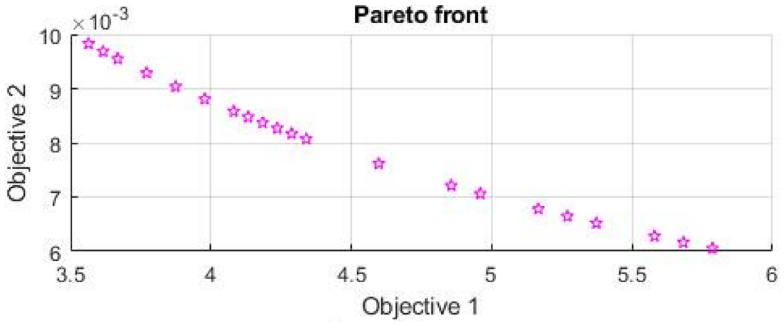

(d) Pareto optimal front for Level –III CFRP nanocomposite laminate for Max stress Th

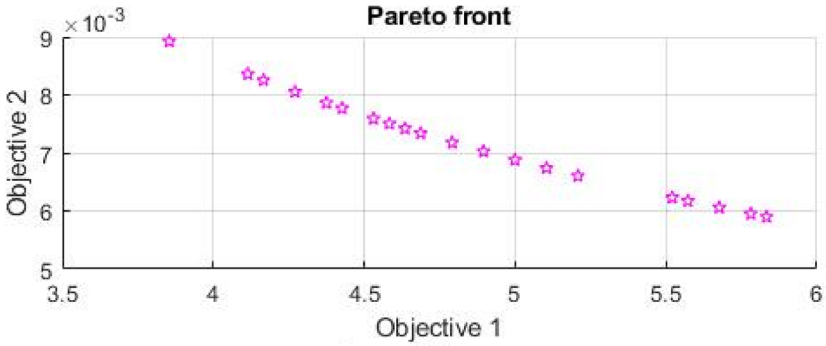

(e) Pareto optimal front for Level –IV CFRP nanocomposite laminate for Max stress Th

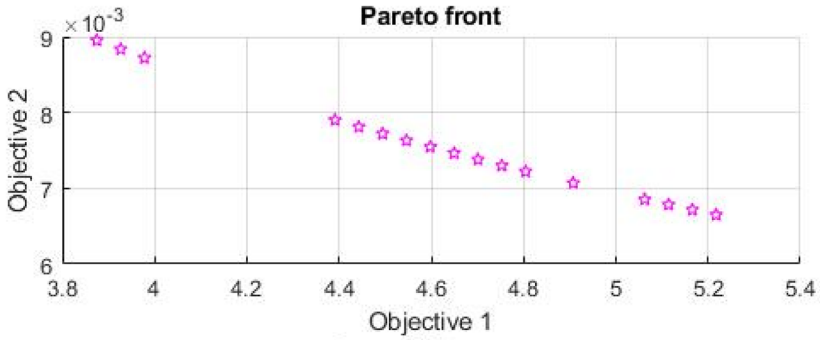

(f) Pareto optimal front for Level –V CFRP nanocomposite laminate for Max stress Th

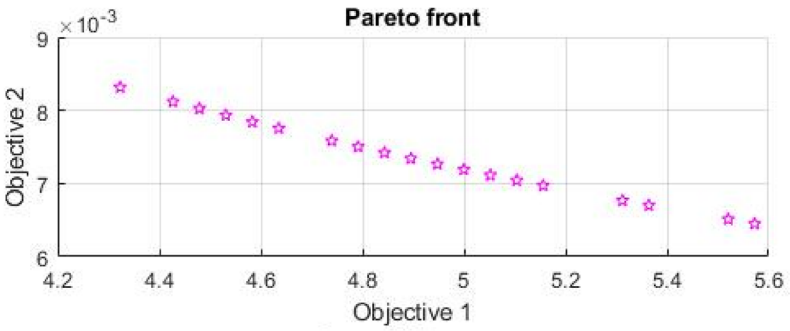

(g) Pareto optimal front for Level –VI CFRP nanocomposite laminate for Max stress Th

Fig. 9 (continued)

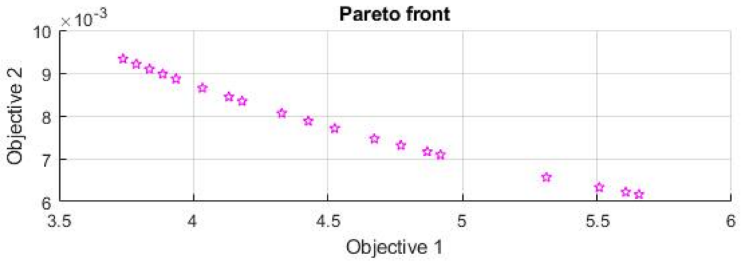

(a) Pareto optimal front for Pure CFRP composite laminate for Tsai-Wu Th

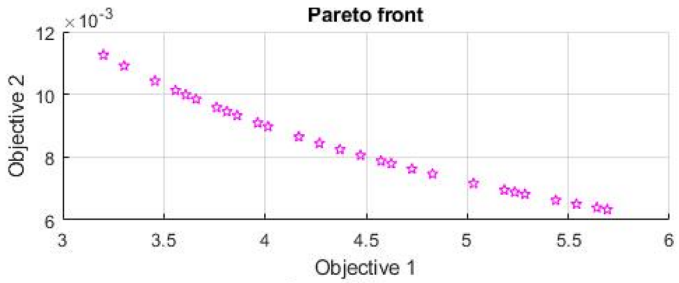

(b) Pareto optimal front for Level –I CFRP nanocomposite laminate for Tsai-Wu Th

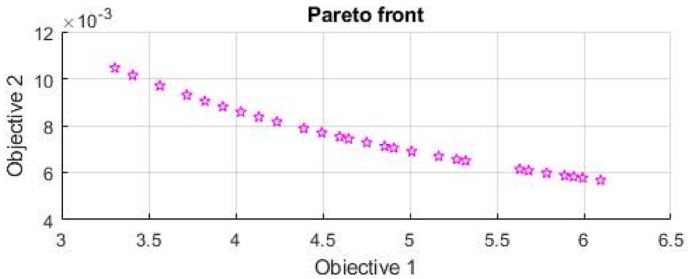

(c) Pareto optimal front for Level –II CFRP nanocomposite laminate for Tsai-Wu Th

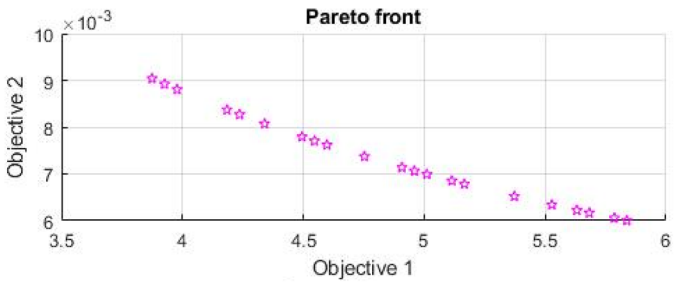

(d) Pareto optimal front for Level –III CFRP nanocomposite laminate for Tsai-Wu Th

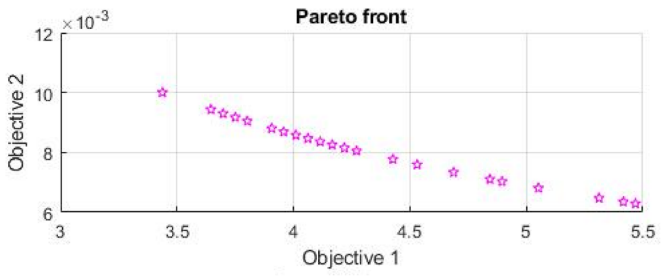

(e) Pareto optimal front for Level –IV CFRP nanocomposite laminate for Tsai-Wu Th

Fig. 10 **a**–**g** Pareto optimal front for various levels of CFRP hybrid nanocomposite for Tsai-Wu theory as a constraint. **a** Pareto optimal front for Pure CFRP composite laminate for Tsai-Wu Th. **b** Pareto optimal front for Level-I CFRP nanocomposite laminate for Tsai-Wu Th. **c** Pareto optimal front for Level-II CFR nanocomposite laminate for Tsai-Wu Th. **d** Pareto optimal front for Level-III CFRP nanocomposite laminate for Tsai-Wu Th. **e** Pareto optimal front for Level-IV CFRP nanocomposite laminate for Tsai-Wu Th. **f** Pareto optimal front for Level-V CFRP nanocomposite laminate for Tsai-Wu Th. **g** Pareto optimal front for Level-VI CFRP nanocomposite for Tsai-Wu Th

Fig. 10 (continued)

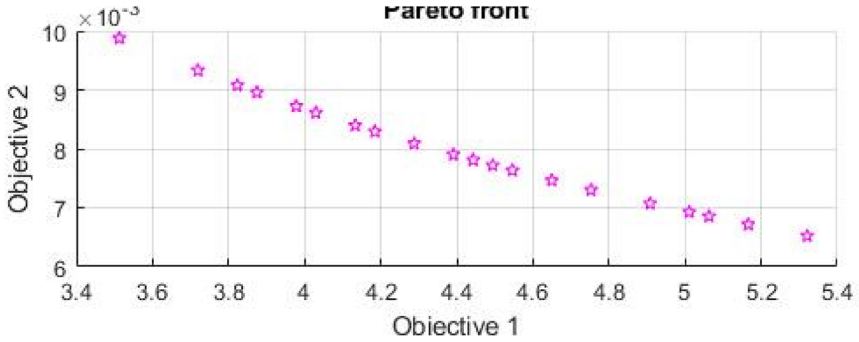

(f) Pareto optimal front for Level –V CFRP nanocomposite laminate for Tsai-Wu Th

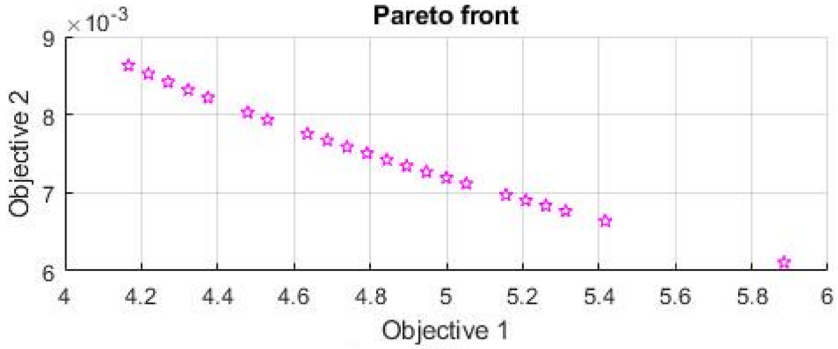

(g) Pareto optimal front for Level –VI CFRP nanocomposite for Tsai-Wu Th

Table 5 Showing samples of stacking sequence angles and thickness of laminates for Max. Stress theory as a constraint

wt% of nanoZnO	wt% of nanoclay	CFRP/Nano mat Combination	Sample stacking sequence angle for max stress theory as a constraint	Sample thickness of laminates for Max stress theory as a constraint
0	0	Pure CFRP	$[0,0,0]_s$, $[0,0,0]_s$, $[0,0,0]_s$	[0.38,0.34,0.35,]s[0.27,0.24,0.3]s[0.36,0.36,0.3]s]
2	2	Level I	$[0,0,0]_s$, $[0,0,0]_s$, $[0,0,0]_s$	[0.37,0.22,0.38]s[0.37,0.22,0.38]s[0.31,0.39,0.36]s
2	3	Level II	$[0,0,0]_s$, $[0,0,0]_s$, $[0,0,0]_s$	[0.3,0.23,0.24]s[0.3,0.23,0.23]s[0.39,0.23,0.23]s
3	2	Level III	$[0,0,0]_s$, $[0,0,0]_s$, $[0,0,0]_s$	[0.29,0.22,0.24]s[0.36,0.36,0.4]s[0.23,0.22,0.24]s
3	3	Level IV	$[0,0,0]_s$, $[0,0,0]_s$, $[0,0,0]_s$	[0.28,0.33,0.39]s[0.28,0.33,0.37]s[0.21,0.3,0.29]s
2	4	Level V	$[0,0,0]_s$, $[0,0,0]_s$, $[0,0,0]_s$	[0.23,0.3,0.39]s[0.23,0.3,0.38]s[0.23,0.3,0.33]s
4	2	Level VI	$[0,0,0]_s$, $[0,0,0]_s$, $[0,0,0]_s$	[0.3,0.33,0.28]s[0.33,0.27,0.35]s[0.31,0.36,0.25]s

Table 6 Showing samples of stacking sequence angles and thickness of laminates for Tsai-Wu Theory as a constraint

wt% of nanoZnO	wt% of nanoclay	CFRP/Nano mat combination	Sample stacking sequence angle for Tsai-Wu theory as a constraint	Sample thickness of laminates for Tsai-Wu theory as a constraint
0	0	Pure CFRP	$[0,0,0]_s$, $[0,0,0]_s$, $[0,0,0]_s$	[0.26,0.24,0.23]s[0.28,0.24,0.23]s[0.36,0.38,0.4]s
2	2	Level I	$[0,0,0]_s$, $[0,0,0]_s$, $[0,0,0]_s$	[0.25,0.33,0.3]s[0.2,0.2,0.24]s[0.21,0.2,0.22]s
2	3	Level II	$[0,0,0]_s$, $[0,0,0]_s$, $[0,0,0]_s$	[0.39,0.39,0.38]s[0.39,0.39,0.4]s[0.23,0.21,0.38]s
3	2	Level III	$[0,0,0]_s$, $[0,0,0]_s$, $[0,0,0]_s$	[0.26,0.27,0.39]s[0.3,0.3,0.22]s[0.3,0.3,0.4]s
3	3	Level IV	$[0,0,0]_s$, $[0,0,0]_s$, $[0,0,0]_s$	[0.25,0.2,0.32,]s[0.25,0.2,0.28]s[0.25,0.2,0.3]s
2	4	Level V	$[0,0,0]_s$, $[0,0,0]_s$, $[0,0,0]_s$	[0.39,0.23,0.35]s[0.2,0.22,0.38]s[0.31,0.36,0.25]s
4	2	Level VI	$[0,0,0]_s$, $[0,0,0]_s$, $[0,0,0]_s$	[0.35,0.27,0.39]s[0.21,0.39,0.21]s[0.24,0.27,0.32]s

References

1. Mohammadi D et al (2015) A multilevel approach for analysis and optimization of nano-enhanced composite structures. Compos Struc 131:1050–1059
2. Taha MR et al (2009) A multi-objective optimization approach for the design of blast-resistantcomposite laminates using carbon nanotubes. Composites B 40:522–529
3. Zhu X et al (2015) An optimization technique for the composite strut using Genetic Algorithms. Mater Des 65:482–488
4. Alemi-Ardakani M et al (2015) A rapid approach for prediction and discrete lay-up optimization of glass fiber/polypropylene composite laminates under the impact. Int J Impact Eng 84:34–144
5. Paluch B et al (2008) Combining a finite element program and a genetic algorithm to optimize composite structures with variable thickness. Compos Struct 83:284–294
6. Almeida F et al (2009) Design optimization of composite laminated structures using genetic algorithms and finite element analysis. Compos Struct 88:443–454
7. Kim D-H et al (2015) Design optimization and manufacture of hybrid glass/carbon fiber reinforced composite bumper beam for automobile vehicle. Compos Struct 131:742–752
8. Kim D-H et al (2014) Design optimization of a carbon fiber reinforced composite automotive lower arm. Composites B 58:400–407
9. Nelson S et al (2016) (2016) Composite laminate failure parameter optimization through four points flexure experimentation and analysis. Composites B 97:92–102
10. Naik N et al (2008) Design optimization of composites using genetic algorithms and failure mechanism based failure criterion. Compos Struct 83:354–367
11. Sohouli M et al (2017) Design optimization of thin-walled composite structures based on material and fiber orientation. Compos Struct. https://doi.org/10.1016/j.compstruct.2017.06.030
12. Rostamiyan Y et al (2015) Experimental and optimizing flexural strength of epoxy-based nanocomposite: effect of using nano-silica and nano clay by using response surface design methodology. Mater Des 69:96–104
13. Rostamiyan Y et al (2015) Experimental, modeling, and optimization study on the mechanical properties of epoxy/high impact polystyrene/multi-walled carbon nanotubes ternary nanocomposite using artificial neural network and genetic algorithm. Mater Des 65:1236–1244
14. Rostamiyan Y et al (2015) Using response surface methodology for modeling and optimizing tensile and impact strength properties of fiber orientated quaternary hybrid nanocomposite. Composites B 69:304–316
15. Chang BP et al (2014) Comparative study of wear performance of particulate and fiber-reinforced nano-ZnO/ultra-high molecular weight polyethylene hybrid composites using response surface methodology. Mater Des 63:805–819
16. Boroujeni AY et al (2014) Hybrid carbon nanotube–carbon fiber composites with improved in-plane mechanical properties. Composites B 66:475–483
17. Mirmohseni A et al (2011) Modelling and optimization of a new impact-toughened epoxy nanocomposite using response surface methodology. Polym Res 18:509–517
18. Shrivastava S et al (2018) Multi-objective multi-laminate design and optimization of a carbon fibre composite wing torsion box using evolutionary algorithm. Compos Struct 185:132–147
19. MarianN. Velea. et al (2014) Multi-objective optimization of vehicle bodies made of FRP sandwich structures. Compos Struct 111:75–84
20. Shojaeefard et al (2014) Multi-objective Optimization of a CNT/Polymer Nanocomposite Automotive Drive Shaft. In: The 3rd International Conference on Design Engineering and Science, ICDES 2014 Pilsen, Czech Republic, August 31–September 3, pp 92–99.
21. Pelletier J (2006) Multi-objective optimization of fiber reinforced composite laminates for strength, stiffness and minimal mass. Comput Struct 84:2065–2080
22. Kalantari M et al (2016) Multi-objective robust optimization of unidirectional carbon/glass fibre reinforced hybrid composites under flexural loading. Compos Struct 138:264–275
23. Irisarr FX et al (2009) Multiobjective stacking sequence optimization for laminated composite structures. Compos Sci Technol 69:983–990
24. De Munck M et al (2015) Multi-objective weight and cost optimization of hybrid composite-concrete beams. Compos Struct 134:369–377
25. Naik N et al (2011) Nature-inspired optimization techniques for the design optimization of laminated composite structures using failure criteria. Exp Syst Appl 38:2489–2499
26. Rahul D et al (2005) Optimization of FRP composites against impact-induced failure using island model parallel genetic algorithm. Compos Sci Technol 65:2003–2013
27. Lopez RH et al (2009) Optimization of laminated composites considering different failure criteria. Composites B 40:731–740
28. Chow WS et al (2008) Optimization of process variables on flexural properties of epoxy/organo-montmorillonite nanocomposite by response surface methodology. Exp Polym Lett 2(1):2–11
29. Nik MA et al (2014) Optimization of variable stiffness composites with embedded defects induced by automated fiber placement. Compos Struct 107:160–166
30. Fe J et al (2018) Optimizing fiber/matrix interface by growth MnO nanosheets for achieving desirable mechanical and tribological properties. Appl Surf Sci 452:364–371
31. Balachandran M et al (2012) Optimizing properties of nanoclay–nitrile rubber (NBR) composites using Face Centred Central Composite Design. Mater Des 35:854–862
32. Abilash et al (2016) Optimizing the delamination failure in bamboo fiber reinforced polyester composite. J King Saud Univ 28:92–102
33. Erdal O et al (2005) Optimum design of composite laminates for maximum buckling load capacity using simulated annealing. Compos Struct 71:45–52
34. Akbulut M et al (2008) Optimum design of composite laminates for minimum thickness. Comput Struct 86:1974–1982
35. Park CH et al (2004) Simultaneous optimization of composite structures considering mechanical performance and manufacturing cost. Compos Struct 65:117–127
36. Srinivas V (2020) Effect of ultrasonic stir casting technique on mechanical and tribological properties of aluminium–multi-walled carbon nanotube nanocomposites. J Bio Tribo corrosion article no. 30, Feb 2020
37. Tripathi VK et al (2019) Manufacturing cost-effective weight minimization of composite laminate using uniform thickness and variable thickness approaches considering different failure criteria. Compos Struct. https://doi.org/10.1007/s41939-019-00048
38. Kulkarni N, Tripathi VK (2019) Buckling load maximization of composite laminate using a random search algorithm considering the uniform thickness and variable thickness approach. J Eng Sci Technol 14(3):1330–1343
39. Kulkarni N, Tripathi VK (2018) Variable thickness approach for finding minimum laminate thickness and investigating the effect of different design variables on its performance. Arch Mech Eng. https://doi.org/10.24425/ame.2018.125441

40. Vo-Duy T et al (2016) A global numerical approach for lightweight design optimization of laminated composite plates subjected to frequency constraints. Compos Struct. https://doi.org/10.1016/j.compstruct.2016.09.059
41. Fakhri LA et al (2018) Optimization of mechanical and color properties of polystyrene/nanoclay/nanoZnO based nanocomposite packaging sheet using response surface methodology. Food Packag Shelf Life 17:11–24
42. Balaji L et al (2020) Study on mechanical, thermal and morphological properties of banana fiber-reinforced epoxy composites. J Bio Tribo corrosion article no. 60, April 2020